Fundamental structure of steady plastic shock waves in metals

A. Molinari
Laboratoire de Physique et Mécanique des Matériaux, ISGMP, Université de Metz, Ile du Saulcy, Metz 57000 Cedex 1, France

G. Ravichandran[a)]
Graduate Aeronautical Laboratories, California Institute of Technology, Pasadena, California 91125

(Received 16 June 2003; accepted 20 November 2003)

The propagation of steady plane shock waves in metallic materials is considered. Following the constitutive framework adopted by R. J. Clifton [*Shock Waves and the Mechanical Properties of Solids*, edited by J. J. Burke and V. Weiss (Syracuse University Press, Syracuse, N.Y., 1971), p. 73] for analyzing elastic–plastic transient waves, an analytical solution of the steady state propagation of plastic shocks is proposed. The problem is formulated in a Lagrangian setting appropriate for large deformations. The material response is characterized by a quasistatic tensile (compression) test (providing the isothermal strain hardening law). In addition the elastic response is determined up to second order elastic constants by ultrasonic measurements. Based on this simple information, it is shown that the shock kinetics can be quite well described for moderate shocks in aluminum with stress amplitude up to 10 GPa. Under the later assumption, the elastic response is assumed to be isentropic, and thermomechanical coupling is neglected. The model material considered here is aluminum, but the analysis is general and can be applied to any viscoplastic material subjected to moderate amplitude shocks. Comparisons with experimental data are made for the shock velocity, the particle velocity and the shock structure. The shock structure is obtained by quadrature of a first order differential equation, which provides analytical results under certain simplifying assumptions. The effects of material parameters and loading conditions on the shock kinetics and shock structure are discussed. The shock width is characterized by assuming an overstress formulation for the viscoplastic response. The effects on the shock structure of strain rate sensitivity are analyzed and the rationale for the J. W. Swegle and D. E. Grady [J. Appl. Phys. **58**, 692 (1985)] universal scaling law for homogeneous materials is explored. Finally, the ability to deduce information on the viscoplastic response of materials subjected to very high strain rates from shock wave experiments is discussed. [DOI: 10.1063/1.1640452]

I. INTRODUCTION

The analysis of plastic shock waves has been the object of numerous studies starting in the years 1942–1945 coinciding with the Manhattan project. A review of this early work is given by Rice *et al.*[1] Of particular interest are the plate impact experiments which provide valuable information on the response of materials upon compressive shock loading. A key result is the Hugoniot diagram, also called the equation of state which relates the compressive stress to the specific volume. Extensive studies have been conducted, and, Hugoniot diagrams have been obtained for a large variety of materials (see Marsh).[2]

For a certain range of shock amplitudes, two compressive shock waves are generated in metallic materials. The first shock is the elastic precursor which compresses the material to the elastic limit. The state reached at the rear of the elastic precursor will be referred to as state $(+)$ in the following. The elastic precursor is followed by the plastic wave, which further compresses the material to the final state, referred to as state $(-)$. The transition from state $(+)$ to state $(-)$ occurs within a thin layer (the plastic shock front) where the material is rapidly deformed. For loadings of large amplitude, steady plastic shocks are observed. In this circumstance the shock front [where the transition from state $(+)$ to state $(-)$ occurs] propagates with a constant velocity and with a constant shape. These steady profiles result from the balance between front steepening due to non-linearity of the material response and smoothing due to dissipation. Steady wave shocks have been first analyzed in Newtonian fluids by Rayleigh[3] and Taylor,[4] and in viscoelastic solids by Band,[5] Band and Duvall,[6] and Bland.[7] In solids, the role of viscous like effects on the shock structure (or profile) has been experimentally identified in the 1960s by Barker,[8] Mineev and Savinov,[9] Mineev and Zaidel,[10] Johnson and Barker,[11] Manvi *et al.*;[12] see also Swan *et al.*,[13] Prieto and Renero,[14] and the summary on this subject by Godounov *et al.*[15]

Plastic shock structures have been analyzed, with the perspective of understanding how shock profiles are affected by the material viscous response. In particular, Johnson and Barker[11] and Swegle and Grady[16] have analyzed experimental recordings where the particle velocity at the rear of the plastic shock is reported in terms of time. They have discussed the effect of the strain rate sensitivity on steady plastic shock profiles. According to Bland,[7] steady plastic shocks

a)Author to whom correspondence should be addressed; electronic mail: ravi@caltech.edu

can be observed when the propagation thickness is larger than five times the plastic shock front thickness. Swegle and Grady[16] analyzed steady plastic shock fronts for a variety of materials and modeled the experiments by using Hugoniot diagrams reported in the literature. For the purpose of analyzing the shock structure, they assumed a specific form of the viscoplastic material response. The wave analysis is made with a finite difference numerical code. An important result is the relationship obtained between the stress jump $\Delta\sigma$ across the shock front and a measure of the strain rate within the shock layer $\dot{\epsilon}_{SG}$ defined as the maximum time derivative of the particle velocity divided by the steady-wave shock velocity. From the analysis of experimental data, they found that for the materials considered, $\dot{\epsilon}_{SG}$ could be related to the stress jump $\Delta\sigma$ by an empirical power law $\dot{\epsilon}_{SG}=\beta(\Delta\sigma)^{h_{SG}}$ with $h_{SG}=4$. In their modeling of shock wave experiments, the exponent h_{SG} is related to the strain rate sensitivity m by the relationship $h_{SG}=2/m$. From these results, it can be concluded that all materials tested exhibit almost the same strain rate sensitivity $m=0.5$ for the deformation (strain rate) regime encountered in the shock experiments considered.

In this article, the problem of the propagation of steady plastic shock waves is revisited. The goal is to provide a further understanding of the relationship between steady plastic shocks, material parameters (strain rate sensitivity, etc.) and loading conditions. In particular, the role of viscous effects on the shock structure will be analyzed in detail. The general problem of compressive plane shock waves in metallic materials is considered. For illustration purposes, aluminum is chosen as the reference material. The constitutive framework used in this paper is similar to the one specified by Clifton[17] in his analysis of transient elasto–plastic waves in aluminum. The problem is formulated in a Lagrangian setting suitable for large deformations. The material response is characterized by a quasistatic tensile (or compression) test which provides in particular the strain hardening law in isothermal conditions. In addition the elastic response is characterized by ultrasonic measurements, up to second order elastic constants. Following Clifton,[17] it is assumed that the deformation process is quasiisentropic, for shocks of moderate amplitudes, and the temperature effects are neglected. Thermomecanical coupling which could have important effects for very strong shocks, can be easily included by keeping the essential structure of the proposed solution. Working within this simplified framework, an analytical solution for steady plastic waves is proposed. This approach seems to be sufficient to get accurate results for shocks of moderate strength (up to 10 GPa for aluminum). The model is validated by comparing the shock velocity, the particle velocity and the shock profiles with available experimental data. It should be emphasized that these results are obtained without using the Hugoniot data. In fact, it is shown that essential features of the Hugoniot diagram for moderate shock amplitudes can be directly retrieved from the present analysis. Surprisingly, the results remain fairly reasonable even for shock amplitudes much larger than 10 GPa.

Most of the solution is given in analytical form and hence provides a clear insight in to the problem. The shock structure is obtained by quadrature of a first order differential equation, made explicit under certain simplifying assumptions, and leading therefore to a closed form solution for steady plastic shocks. The effects of material parameters and loading conditions on the shock kinetics and shock structure are discussed. The shock width is also characterized in explicit form. Assuming an overstress formulation for the visco–plastic flow law (Perzyna),[18] the effects of the strain rate sensitivity and of material hardening on the shock structure are analyzed. The relationship between the stress jump and the intensity of plastic strain rate within the shock layer is established. As in the work of Swegle and Grady,[16] this relationship is shown to be well described by a power law. The exponent of this power law depends on the strain rate sensitivity and this dependence is formulated in explicit form. The results are compared to those of Swegle and Grady.[16] Finally, a methodology for obtaining information on the viscoplastic response of materials subjected to very high strain rates using the shock waves experiments is discussed.

II. KINEMATIC AND CONSTITUTIVE FRAMEWORK

Consider a plane shock wave moving in the positive x direction. The displacement of a material particle has a component u in the x direction, the components being zero along the y and z directions of the orthonormal frame $Oxyz$ (with unit vector basis $\mathbf{e}_1$, $\mathbf{e}_2$, and $\mathbf{e}_3$), corresponding to uniaxial strain. The problem is formulated in a Lagrangian setting appropriate for large deformation. The kinematical and constitutive framework proposed by Clifton[17] in his analysis of transient elastic–plastic waves is closely followed. The wave amplitudes considered were of moderate intensity and the process was treated as quasiisentropic.

A. Kinematics

X denotes the Lagrangian coordinate of a particle in the initial state, x the current position, and by u the longitudinal displacement: $x=X+u(X)$. The deformation gradient has the form

$$\mathbf{F}=\lambda_1\mathbf{e}_1\otimes\mathbf{e}_1+\mathbf{e}_2\otimes\mathbf{e}_2+\mathbf{e}_3\otimes\mathbf{e}_3 \tag{1}$$

where the longitudinal stretch is defined by

$$\lambda_1=\frac{\partial x}{\partial X}=1+\frac{\partial u}{\partial X}=\frac{V}{V_0};$$

where V and V_0 are, respectively, the current and the reference volumes of a material element. The deformation gradient can be decomposed in to elastic (e) and plastic (p) parts through the standard multiplicative decomposition

$$\mathbf{F}=\mathbf{F}^e\mathbf{F}^p \tag{2}$$

with

$$\mathbf{F}^e=\lambda_1^e\mathbf{e}_1\otimes\mathbf{e}_1+\lambda_2^e\mathbf{e}_2\otimes\mathbf{e}_2+\lambda_2^e\mathbf{e}_3\otimes\mathbf{e}_3, \tag{3}$$

$$\mathbf{F}^p=\lambda_1^p\mathbf{e}_1\otimes\mathbf{e}_1+\lambda_2^p\mathbf{e}_2\otimes\mathbf{e}_2+\lambda_2^p\mathbf{e}_3\otimes\mathbf{e}_3. \tag{4}$$

The axes y and z play equivalent roles, therefore the stretches in the y and z directions are identical as formulated in Eq.

(3). From Eq. (2), the total stretches are the products of elastic and plastic stretches; using in addition Eq. (1), it follows that

$$\lambda_1=\lambda_1^e\lambda_1^p \quad \lambda_2=\lambda_3=\lambda_2^e\lambda_2^p=1. \tag{5}$$

Using plastic incompressibility

$$\det \mathbf{F}^p=1 \tag{6}$$

one obtains

$$\lambda_1^e=\lambda_1/\lambda_1^p, \quad \lambda_2^e=(\lambda_1^p)^{1/2}, \quad \lambda_2^p=(\lambda_1^p)^{-1/2}. \tag{7}$$

and all the stretches can then be expressed in terms of the total (λ_1) and plastic (λ_1^p) stretches in the direction of wave propagation.

B. Constitutive equations

In this section, the basic governing equations of the problem are introduced. The Lagrangian form of the equation of conservation of linear momentum is

$$\frac{\partial T_1}{\partial X}=\rho_0\frac{\partial v}{\partial t}, \tag{8}$$

where t is time, $v=\partial u(X,t)/\partial t$ is the particle velocity, ρ_0 is the mass density in the reference configuration, and T_1 is the component of the Piola–Kirchhoff stress tensor in the wave propagation direction (force per unit area in the reference configuration). Using axisymmetry, the stress tensor can be expressed in the form

$$\mathbf{T}=T_1\mathbf{e}_1\otimes\mathbf{e}_1+T_2\mathbf{e}_2\otimes\mathbf{e}_2+T_2\mathbf{e}_3\otimes\mathbf{e}_3. \tag{9}$$

Note that T_1 coincides with the component σ_1 of the Cauchy stress tensor, because a material surface element normal to the propagation direction remains unchanged during the process. However, the transverse stress component T_2 is different from σ_2.

The kinematic compatibility equation has the form

$$\frac{\partial v}{\partial X}=\frac{\partial \lambda_1}{\partial t}. \tag{10}$$

The conditions where the temperature variation can be neglected are considered here. Therefore, the equation of conservation of energy is not needed here.

The elastic constitutive law for an isentropic process can be written as[17]

$$T_1=(\rho_0/\lambda_1^p)F_1(\epsilon_1^e,\epsilon_2^e), \tag{11}$$

$$T_2=\rho_0(\lambda_1^p)^{1/2}F_2(\epsilon_1^e,\epsilon_2^e). \tag{12}$$

The elastic components of the strain tensor are given by

$$\epsilon_1^e=\lambda_1^e-1=(\lambda_1/\lambda_1^p)-1, \tag{13}$$

$$\epsilon_2^e=\lambda_2^e-1=(\lambda_1^p)^{1/2}-1. \tag{14}$$

The functions F_1 and F_2 specified in Appendix A, are second order polynomials with respect to elastic deformations. The second order thermoelastic constants are traditionally obtained using ultrasonics measurements. In view of the relationships Eqs. (13) and (14), the stress components are solely dependent upon the stretches λ_1 and λ_1^p.

The viscoplastic flow rule has the following functional form [see Eq. (38) in Ref. 17]

$$\frac{\dot{\lambda}_1^p}{\lambda_1^p}=-\frac{2}{3}\Phi(\tau,\gamma^p). \tag{15}$$

τ is the maximum shear stress, which in the current configuration is given by

$$\tau=1/2(T_1-T_2/\lambda_1). \tag{16}$$

The hardening parameter γ^p is a measure of the plastic shear strain defined as

$$\gamma^p=\int \Phi\, dt=-3/2\ln(\lambda_1^p). \tag{17}$$

Note that Φ is in general temperature dependent, but the temperature effect is neglected here. The form adopted for Φ is as follows:

$$\Phi=bN\overline{\nu}, \tag{18}$$

where b is a constant (in a single crystal b can be identified with the length of the Burgers vector associated with single slip); $N=N(\gamma^p)$ is the mobile dislocation density, a function of the cumulated plastic strain. Following Johnson and Barker,[11] the following form is adopted:

$$N=N_{m0}[1+(\alpha_b\gamma^p/bN_{t0})]\exp(-\alpha_t\alpha_b\gamma^p), \tag{19}$$

where N_{m0} is the initial mobile dislocation density, N_{t0} is the initial total dislocation density, α_b is the breeding coefficient, and α_t is the trapping coefficient. Values of these parameters are specified for aluminum in Table I. The average dislocation velocity $\overline{\nu}=\overline{\nu}(\tau,\gamma^p,\theta)$ is in general dependent upon the resolved stress τ, the accumulated plastic strain γ^p, and the temperature θ. The temperature dependence shall not be considered here.

The stress dependence of $\overline{\nu}$ is assumed to be described by an overstress model. In this theory, viscoplastic flow occurs when the resolved stress τ is exterior to the elastic domain ($|\tau|>\tau_a$) and vanishes otherwise ($|\tau|\leqslant\tau_a$), with τ_a being the yield stress in pure shear. Strain hardening is described in terms of γ^p by the following power law:

$$\tau_a=\tau_{a0}\left[1+\left(\frac{\gamma^p}{\gamma_0}\right)^{1/n}\right], \tag{20}$$

where τ_{a0}, γ_0, and n are material parameters that can be obtained from quasistatic tests (see Table I). Ideally, it would be better to use data obtained from adiabatic tests, since these data will include thermal softening effects due to the self-heating produced by plastic dissipation. However, this modification would just slightly influence the results for plastic shock waves of moderate amplitude. The reason is that for small strains the heat produced by dissipation is small enough that can be neglected. For larger strains, τ_a could be affected by thermal softening, but then the compressive stress σ becomes large with respect to τ_a and knowing the precise value of τ_a is of not significant importance.

Under compressive loading τ is negative, and the yield condition is

$$\tau+\tau_a=0. \tag{21}$$

TABLE I. Material parameters for 6061-T6 aluminum at room temperature (25 °C) and atmospheric pressure.

$\rho_0 = 2703\ \mathrm{kg/m^3}$	(mass density)
$c_L = 6368\ \mathrm{m/s}$	(longitudinal wave speed)
$c_S = 3197\ \mathrm{m/s}$	(shear wave speed)
Elastic Constants	
$a_2 = c_L^2/2 = 20.28\times10^6\ (\mathrm{m/s})^2$; $a_3 = -2c_S^2 = -20.44\times10^6\ (\mathrm{m/s})^2$; $a_4 = -66.4\times10^6\ (\mathrm{m/s})^2$; $a_5 = 157.5\times10^6\ (\mathrm{m/s})^2$; $a_6 = -142.8\times10^6\ (\mathrm{m/s})^2$	
Plastic characteristics provided by a quasistatic tensile test (hardening law [Eq. (20)])	
$\tau_{a0} = 120\ \mathrm{MPa}$	(initial back stress)
$\gamma_0 = 0.52$	(reference strain)
$n = 1.55$	(hardening parameter)
Conjectured viscoplastic properties (see [Eqs. (19) and (23)])	
$M = 1/m = 1.78$	(m is the strain rate sensitivity)
$c_1 = 0.168\ \mathrm{ms^{-1}}$	
$T_1^* = 1.6\ \mathrm{MPa}$	
$b = 0.286\times10^{-9}\ \mathrm{m}$	(lattice parameter constant)
$N_{m0} = 0.818\times10^{13}\ \mathrm{m^{-2}}$	(initial mobile dislocation density)
$N_{t0} = 0.818\times10^{13}\ \mathrm{m^{-2}}$	(initial total dislocation density)
$\alpha_b = 3.5\times10^5\ \mathrm{m^{-1}}$	(breeding coefficient)
$\alpha_t = 0$	(trapping coefficient)
Thermomechanical parameters	
$b_1 = -593\ \mathrm{K}$; $b_2 = -130\ \mathrm{K}$; $b_3 = 1350\ \mathrm{K}$	
$c_p = 908\ \mathrm{J(K\,g)^{-1}\,(K)^{-1}}$	(heat capacity at constant pressure)
$\beta = 0.9$	(Taylor–Quinney coefficient)

[a]Adapted from Ref. 17.

Viscoplastic flow occurs when

$$\tau + \tau_a < 0. \tag{22}$$

It is assumed that $\overline{\nu}$ is a power law function of the overstress

$$\overline{\nu} = c_1 \left(\frac{|\tau + \tau_a|}{T_1^*} \right)^M, \tag{23}$$

where c_1 and T_1^* are material constants, and $M = 1/m$ is the inverse of the strain rate sensitivity m. The following values will be used $c_1 = 0.168\ \mathrm{ms^{-1}}$, $M = 1.78$, and $T_1^* = 1.6\ \mathrm{MPa}$. Clifton[17] and Johnson and Barker[11] have used a slightly different form

$$\overline{\nu} = c_s \left(\frac{|\tau + \tau_a|}{T^*} \right)^{M_c}, \tag{24}$$

with $M_c = 2.14$, $c_s = 3197\ \mathrm{m/s}$, and $T^* = 203\ \mathrm{MPa}$. Note that Eq. (23) would coincide with Eq. (24) for $M = M_c$ and $T_1^* = 2.03\ \mathrm{MPa}$.

The choice of the parameters in Table I will be justified later by considering the shock profiles recorded in plate impact experiments. The methodology used to identify these parameters will be discussed in Sec. VI.

Finally the problem of the propagation of steady plastic waves is governed by a system of five equations [Eqs. (8), (10), (11), (12), and (15)], the variables being λ_1, λ_1^p, ν, T_1, and T_2. Furthermore, if T_1, T_2, and τ are expressed in terms of λ_1 and λ_1^p with the use of Eqs. (13), (14), and (16), one obtains, after substitution of these expressions into Eqs. (8) and (15), a system of three equations [Eqs. (8), (10), and (15)] for the unknowns λ_1, λ_1^p, and ν.

The values of the material parameters used in this article for 6061-T6 aluminum are given in Table I; for further information on thermo–elastic properties see Clifton.[17] During the parametric analysis in Sec. VI, some values of the material parameters of Table I will be varied for illustrative purposes.

C. Isothermal compression curve

In Fig. 1(a), the variation of the compressive stress $\sigma = -T_1$ for 6061-T6 aluminum is reported in terms of the total stretch λ_1 for a slow compression process; then viscous effects can be neglected and the stress state remains on the yield surface. In Fig. 1(a), the stretch λ_1 is decreased from the initial value $\lambda_1 = 1$ to $\lambda_1 = 0.9$. The elastic limit is reached at $\lambda_1^+ = 0.995\,78$, for the value $\sigma^+ = 0.473\ \mathrm{GPa}$ of the compressive stress. For $\lambda_1^+ \leqslant \lambda_1 \leqslant 1$, the response is purely elastic and the plastic stretch is equal to $\lambda_1^p = 1$. When the material is further compressed, one enters the elasto–plastic regime ($\lambda_1 < \lambda_1^+$). The resulting stress–stretch response is the slightly convex curve shown in Fig. 1(a) corresponding to states (λ_1, λ_1^p) for which the yield criterion Eq. (21) is satisfied. More precisely, for a given λ_1, the plastic stretch λ_1^p is determined in terms of λ_1 so as to satisfy the yield criterion $\tau(\lambda_1, \lambda_1^p) + \tau_a(\lambda_1^p) = 0$. This relationship defines a correspondence between λ_1 and λ_1^p which can be denoted as

$$\lambda_1^p = f_Y(\lambda_1) \quad \lambda_1 = g_Y(\lambda_1^p). \tag{25}$$

Therefore, the compression curve can be parameterized by λ_1, $\sigma = -T_1(\lambda_1, f_Y(\lambda_1))$. C_Y denotes the elasto–plastic part of the compression diagram. The subscript $(\cdot)_Y$ is used in Eq. (25) to indicate that these relationships are only valid on C_Y.

It is worth noting that the resolved stress τ vanishes if $\lambda_1^p = \lambda_1^{2/3}$. For stress levels large enough so that the threshold stress τ_a can be neglected, the yield criterion can be written

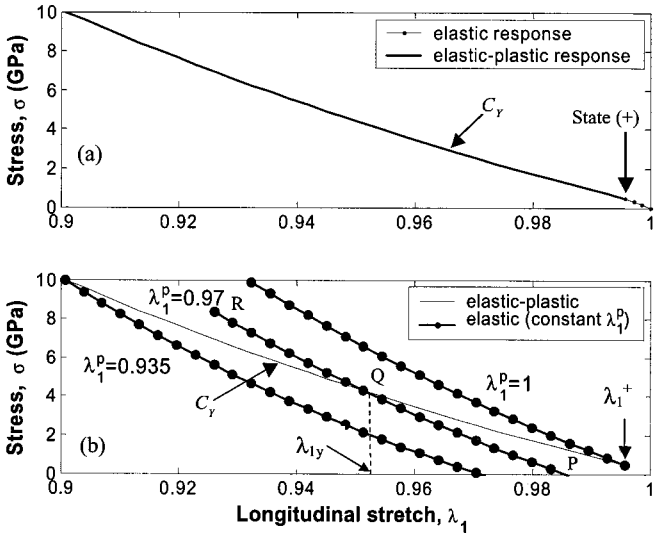

FIG. 1. (a) Compressive stress $\sigma=-T_1$ for 6061-T6 aluminum in terms of the total stretch $\lambda_1=V/V_0$. At the state $(+)$ corresponding to the elastic limit, $\lambda_1^+=0.995\,78$ and $\sigma^+=-T_1^+=0.473$ GPa. The elastic–plastic part of the compression diagram corresponds to $\sigma>\sigma^+$ and is denoted by C_Y. On C_Y, the yield condition $\tau+\tau_a=0$ is satisfied and the relationship $\lambda_1^p=(\lambda_1/\lambda_1^+)^{2/3}$ is verified to a very good approximation. (b) Dashed curves are unloading elastic paths obtained by increasing λ_1 for a fixed value of λ_1^p, illustrating the one-to-one correspondence between points (λ_1,σ) and stretches (λ_1,λ_1^p). λ_{1Y} denotes the stretch at the intersection of C_Y with iso-λ_1^p curves (for instance at Q, $\lambda_{1Y}=0.9512$ for $\lambda_1^p=0.97$). As stated before, to a very good approximation, $\lambda_1^p=(\lambda_{1Y}/\lambda_1^+)^{2/3}$.

as $\tau=0$. Under these conditions, the points (λ_1,σ) on C_Y are associated with the stretches $(\lambda_1,\lambda_1^p=\lambda_1^{2/3})$. Actually, a remarkable fit of the quasistatic compression curve C_Y can be obtained by considering the following approximation of the function f_Y:

$$\lambda_1^p=f(\lambda_1)\approx(\lambda_1/\lambda_1^+)^{2/3}. \tag{26}$$

At the state $(+)$ the condition $\lambda_1^p=1$ is satisfied by Eq. (26). Using Eq. (26) to plot the compression curve produces a result which is indistinguishable from the curve shown in Fig. 1(a).

In Fig. 1(b), the elastic unloading paths obtained by increasing λ_1 for a fixed value of λ_1^p are presented. For instance, the path RQP corresponds to the fixed value of $\lambda_1^p=0.97$. The state Q can be reached by following the "quasistatic" compression curve C_Y. Upon unloading, the elastic path $Q\rightarrow P$ is followed. To attain the state R, a fast loading has to be considered, for which viscous effects allow the stress to be above the curve C_Y (visco–plastic overstress model). Upon rapid unloading, the elastic path $R\rightarrow Q\rightarrow P$ is followed. From Fig. 1(b) it appears that a one to one correspondence can be established between each point of the (λ_1,σ) diagram and the stretches (λ_1,λ_1^p). When stretches (λ_1,λ_1^p) are known, the material state is entirely determined, i.e. all other variables can be calculated (stretches, strains, and stresses: T_1, T_2, τ, τ_a).

III. STEADY STATE SHOCK WAVES

For shocks with large enough amplitude, steady profiles can be achieved. These steady shock profiles propagate without change in form, which results from the balance between the steepening effect of the nonlinear (viscoplastic) material response and the smoothing effect of dissipation. For a certain range of shock amplitudes, two compressive shock waves are generated. The first shock is the elastic precursor, which compresses the material to the elastic limit. The state reached at the rear of the elastic precursor will be referred to as state $(+)$. The corresponding compressive stress, particle velocity, and stretches are, respectively, denoted by $\sigma^+=-T_1^+$, ν^+, λ^+, λ^{p+}. The elastic precursor is followed by a plastic wave, which further compresses the material to the final stress level $\sigma^-=-T_1^-$. The transition from σ^+ to σ^- occurs within the shock front, which is a thin layer where the material is rapidly deformed at very high strain rates. While in the present model, material viscosity does not affect the shape of the compression curve C_Y, viscous effects play a key role in structuring the shock front layer. If viscous effects are neglected, this layer can be idealized as being infinitely thin and the stress sustains an instantaneous jump $\Delta\sigma=\sigma^-\sigma^+$ at the shock front.

A. Basic equations

To model the steady structure of plastic waves, consider an observer moving with the Lagrangian velocity C of the plastic shock with respect to the reference configuration. This velocity is constant for a steady state shock. For this observer, the shock profile has a steady structure and all quantities can be expressed in terms of a moving coordinate

$$\xi=X-Ct. \tag{27}$$

Therefore, Eqs. (8) and (10) can be written as

$$\frac{dT_1}{d\xi}=-C\rho_0\frac{d\nu}{d\xi} \tag{28}$$

$$\frac{d\nu}{d\xi}=-C\frac{d\lambda_1}{d\xi}. \tag{29}$$

The analysis is conducted by considering that the local frame is stretched in the ξ direction so that states $(+)$ and $(-)$ are, respectively, at $\xi=+\infty$ and $\xi=-\infty$. Upon integration with respect to ξ, it follows, for any point within the plastic shock layer

$$T_1-T_1^+=-\rho_0C(\nu-\nu^+), \tag{30}$$

$$\nu-\nu^+=-C(\lambda_1-\lambda_1^+). \tag{31}$$

From Eqs. (30) and (31), it is established that the stress T_1 is linearly related to the stretch λ_1,

$$T_1-T_1^+=\rho_0C^2(\lambda_1-\lambda_1^+). \tag{32}$$

This relationship defines the so called Rayleigh line, a straight line in the (T_1,λ_1) diagram. Considering in particular the state $(-)$, one has

$$T_1^--T_1^+=-\rho_0C(\nu^--\nu^+), \tag{33}$$

$$\nu^--\nu^+=-C(\lambda_1^--\lambda_1^+), \tag{34}$$

$$T_1^--T_1^+=\rho_0C^2(\lambda_1^--\lambda_1^+). \tag{35}$$

The state (+) corresponds to initial yielding, for which plastic deformation is still nonexistent. Thus, at state (+), one has $\lambda_1^{p+}=1$, and the yield condition Eq. (21) takes the form

$$1/2(T_1(\lambda_1^+,1)-T_2(\lambda_1^+,1)/\lambda_1^+)+\tau_{a0}=0. \tag{36}$$

The stretch λ_1^+ is determined as the solution to Eq. (36). The corresponding stress is given by

$$T_1^+=T_1(\lambda_1^+,1). \tag{37}$$

For 6061-T6 aluminum, whose material characteristics are defined in Table I, $\lambda_1^+=0.995\,78$ and $\sigma^+=-T_1^+=473$ MPa. The particle velocity v_1^+ is given by a relationship similar to Eq. (34), where C is replaced by the velocity of the elastic precursor

$$c_{\mathrm{el}}=\sqrt{\frac{\sigma^+}{\rho_0(1-\lambda_1^+)}},\qquad v^+=c_{\mathrm{el}}(1-\lambda_1^+). \tag{38}$$

The following results are obtained for the elastic precursor wave speed and particle velocity:

$$c_{\mathrm{el}}=6434\ \text{m/s}$$

and

$$v^+=27.2\ \text{m/s}.$$

State (−) is entirely determined by a single input parameter characterizing the shock amplitude. This parameter can either be the stress amplitude $\sigma^-=-T_1^-$ or the stretch λ_1^- or the shock velocity C. Assuming for example that λ_1^- is given, the plastic stretch λ_1^{p-} can be calculated by considering the yield condition Eq. (21) at state (−)

$$1/2[T_1(\lambda_1^-,\lambda_1^{p-})-T_2(\lambda_1^+,\lambda_1^{p-})/\lambda_1^-]+\tau_a^-=0 \tag{39}$$

with

$$\tau_a^-=\tau_{a0}\left[1+\left(\frac{-3/2\ln(\lambda_1^{p-})}{\gamma_0}\right)^{1/n}\right]. \tag{40}$$

The stress is given in terms of stretches by

$$\sigma^-=-T_1^-=-T_1(\lambda_1^-,\lambda_1^{p-}). \tag{41}$$

Shock velocity C and particle velocity v_1^- follow from Eqs. (35) and (34). Similar calculations can be made if, in place of λ_1^-, the input parameter is the stress T_1^-.

B. Shock structure

Once the states (+) and (−) are characterized, the shock structure is entirely determined from the flow equation (15), which, by considering Eq. (27), can be expressed as

$$\frac{d\lambda_1^p}{d\xi}=\frac{2\lambda_1^p}{3C}\Phi(\tau,\gamma^p)$$

with

$$\gamma^p=-3/2\ln(\lambda_1^p). \tag{42}$$

In addition, all states within the plastic shock are constrained to be on the Rayleigh line Eq. (32). This constraint provides an equation for determining the plastic stretch λ_1^p in terms of the total stretch λ_1 in the shock layer

$$T_1(\lambda_1,\lambda_1^p)-T_1^+=\rho_0C^2(\lambda_1-\lambda_1^+). \tag{43}$$

Let us denote this functional dependence by

$$\lambda_1=g_R(\lambda_1^p). \tag{44}$$

With the aid of Eqs. (11), (12), (16), and (44), the stress τ can be expressed uniquely in terms of λ_1^p. Finally, considering that γ^p is related to λ_1^p by Eq. (17), Φ appears to be solely the function of λ_1^p,

$$\Phi_R(\lambda_1^p)=\Phi[\tau(\lambda_1^p),\gamma^p(\lambda_1^p)]. \tag{45}$$

The subscript R used in Eqs. (44) and (45) indicates that these relationships are only valid within the shock structure (i.e., on the Rayleigh line). Finally, with Eq. (45), the flow rule Eq. (42) can be written in the form of a first order differential equation with respect to the single unknown λ_1^p

$$\frac{d\lambda_1^p}{d\xi}=\frac{2}{3C}\lambda_1^p\Phi_R(\lambda_1^p). \tag{46}$$

Note that the viscoplastic flow vanishes ($\Phi=0$) at states (+) and (−), i.e., at $\xi=+\infty$ and $\xi=-\infty$, respectively, since the yield criterion Eq. (21) is identically satisfied at these states. The flow equation (46) determines the shock structure.

Within the shock layer, the stretches λ_1 and λ_1^p are related by Eq. (44). A remarkable feature of the present model is that this relationship can be written in an explicit form. As shown in Appendix A, the function $F_1(\epsilon_1^e,\epsilon_2^e)$, involved in the expression Eq. (11) for T_1 is a second order polynomial with respect to the arguments ϵ_1^e and ϵ_2^e

$$F_1(\epsilon_1^e,\epsilon_2^e)=A_1\epsilon_1^e+A_2\epsilon_1^{e^2}+B_1\epsilon_2^e+B_2\epsilon_2^{e^2}+D\epsilon_1^e\epsilon_2^e, \tag{47}$$

with A_1, A_2, B_1, B_2, D given by Eq. (A5). Since $\lambda_1^p=(1+\epsilon_2^e)^2$, the relationship Eq. (32) describing the Rayleigh line provides a second order algebraic equation with respect to ϵ_1^e

$$A_2\epsilon_1^{e^2}+B\epsilon_1^e+G=0 \tag{48}$$

with

$$\begin{aligned}B&=A_1+D\epsilon_2^e-C^2(1+\epsilon_2^e)^4,\\ G&=B_1\epsilon_2^e+B_2\epsilon_2^{e^2}+(C^2\lambda^+-T_1^+/\rho_0)(1+\epsilon_2^e)^2\\ &\quad -C^2(1+\epsilon_2^e)^4,\end{aligned} \tag{49}$$

where C is the velocity of the plastic shock wave. Considering that $\epsilon_2^{e+}=0$ at the state (+), the only root of Eq. (48) having a physical meaning is

$$\epsilon_1^e=\frac{-B+\sqrt{B^2-4A_2G}}{2A_2}. \tag{50}$$

From Eq. (50), ϵ_1^e can be expressed in terms of ϵ_2^e or λ_1^p by

$$\epsilon_1^e=f(\epsilon_2^e)=f[(\lambda_1^p)^{1/2}-1], \tag{51}$$

where the function f has the form

$$f(X)=\frac{-B(X)+\sqrt{(B(X))^2-4A_2G(X)}}{2A_2}. \tag{52}$$

Finally, the explicit form of Eq. (44) is obtained by using Eqs. (13) and (51)

$$\lambda_1=g_R(\lambda_1^p)=\lambda_1^p[1+f((\lambda_1^p)^{1/2}-1)]. \tag{53}$$

Note that the longitudinal plastic strain rate $\dot{\epsilon}^p$ can be written in terms of λ_1^p

$$\dot{\epsilon}^p=\dot{\lambda}_1^p/\lambda_1^p=-(2/3)\Phi_R(\lambda_1^p). \tag{54}$$

Using Eqs. (53), (54), and (3), the total strain rate $\dot{\epsilon}$ can also be expressed in terms of λ_1^p

$$\dot{\epsilon}=\frac{\dot{\lambda}_1}{\lambda_1}=-\frac{2}{3}\lambda_1^p\frac{g_R'(\lambda_1^p)}{g_R(\lambda_1^p)}\Phi_R(\lambda_1^p). \tag{55}$$

The explicit form of the derivative g_R' of g_R with respect to λ_1^p, is given in Appendix B. Integration of the differential equation (46) provides the shock structure, i.e., the variation of λ_1^p with respect to the position ξ. The evolution of the material state with ξ follows, because the material state is characterized by (λ_1,λ_1^p), and λ_1 is related to λ_1^p by Eq. (53).

IV. COMPARISON WITH EXPERIMENTS

In this section, the model predictions are compared with experimental data for aluminum.[1,11]

A. Shock velocity and particle velocity

In Fig. 2, the isothermal compression curve for a shock of stress amplitude $\sigma^-=3.7$ GPa is considered. Points J and K on the compression curve C_Y correspond, respectively, to the states $(+)$ and $(-)$, ahead and at the rear of the plastic shock. According to Eq. (35), the slope of the segment JK is $-\rho_0C^2$. As shown before, the stretches λ_1^- and λ_1^{p-} at K are determined so as to satisfy the yield condition Eq. (21) at the given stress σ^-. The plastic shock velocity C is obtained from Eq. (35) and the particle velocity v^- from Eqs. (33) or (34). The resulting values are: $\lambda_1^-=0.9577$, $\lambda_1^{p-}=0.9745$, $C=5602$ m/s, and $v^-=240$ m/s. Results for $\sigma^-=15$ GPa are shown in Fig. 2(b), and Table II. Other results obtained for a variety of stress amplitudes are compared in Table II to experimental data for aluminum reported by Rice *et al.*[1] and Johnson and Barker.[11]

This comparison shows that for moderate shocks with stress amplitude less than 20 GPa, the present simplified constitutive framework provides quite good information concerning the shock kinematics. Even for much stronger shocks up to 100 GPa, the model predictions remain acceptable. The fact that dissipation and temperature effects can be neglected for moderate shocks is illustrated in Fig. 2. The energy dissipated by viscous effects is proportional to the area between the Rayleigh line and the compression curve C_Y. In addition, one has to consider the energy dissipated by plastic work. For $\sigma^-<20$ GPa, this dissipated energy is not large enough to influence significantly the compressive stress. The temperature rise at the rear of the plastic shock is evaluated in Appendix C.

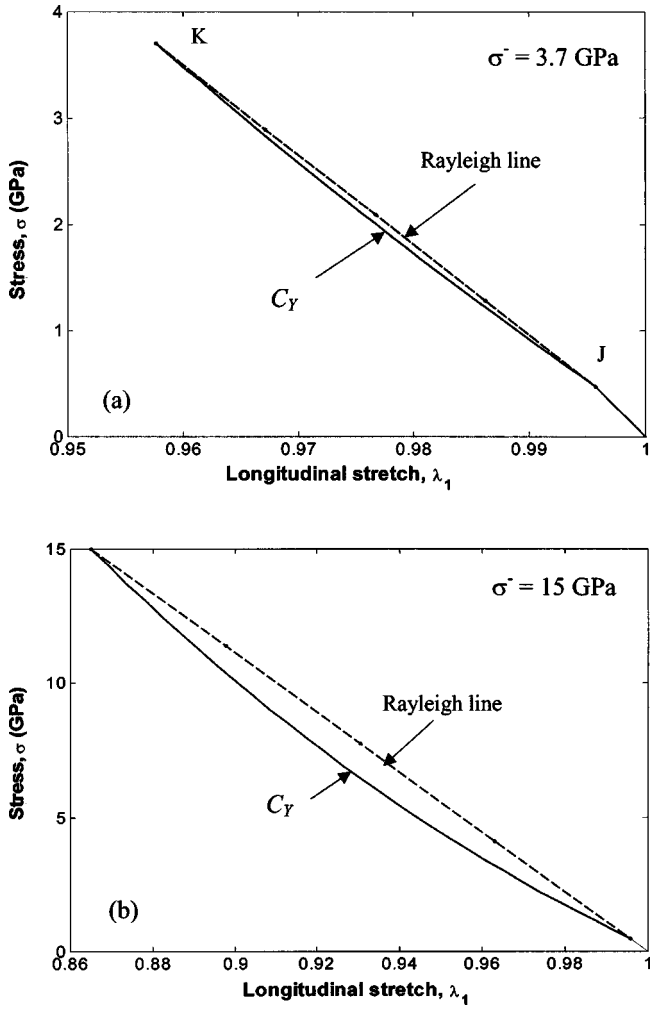

FIG. 2. Compressive stress σ in terms of the stretch $\lambda_1=V/V_0$ for two values of the shock strength σ^-. The Rayleigh line is the segment JK with slope, $-\rho_0C^2$, where C is the plastic shock velocity. The energy dissipation due to viscous effects is proportional to the area between the Rayleigh line and the curve C_Y. Another part of the dissipate energy is due to the plastic work. Note that the dissipation due to viscous effects is very small for the shock amplitude $\sigma^-=3.7$ GPa compared with the total energy involved in the compression process [area under the curve IJK, with $I=(\lambda_1=1,\sigma=0)$ being the origin of the compression curve].

In Fig. 3, the variation of the plastic shock velocity C is given in terms of the particle velocity v^- at the rear of the plastic shock. The range of velocities corresponds to stress amplitudes from 2.1 to 9 GPa (as in Johnson and Barker's[11] experiments). The linear dependence is in agreement with experiments and the predicted slope $S=1.347$ is close to the value $S=1.337$ obtained by Swegle and Grady[16] from the experimental data of Johnson and Barker.[11] The Eulerian value of the shock velocity is given by, (see for instance Swegle and Grady[16])

$$C^{\text{eul}}=v^++c^++S(v^--v^+), \tag{56}$$

where c^+ is the sound velocity associated with the state $(+)$. When the stress amplitude σ^- is decreased to the value σ^+, it follows that $v^-\to v^+$ and $C^{\text{eul}}\to v^++c^+$. Therefore the Lagrangian shock velocity is tending to the value $C=c^+$. Considering the results reported in Fig. 3, one obtains in this

TABLE II. Experimental data for aluminum (Johnson and Barker[a] and Rice, McQueen and Walsh[b]) are compared with the present model. σ^-, ν^-, and $\lambda_1^- = V^-/V_0$ are respectively, the stress, the particle velocity, and the stretch at the rear (steady state) of the plastic shock front.

	Stress amplitude σ^- (GPa)	Plastic shock velocity C (m/s)		Particle velocity ν^- (m/s)		Stretch λ_1^-	
		Expt.	Model	Expt.	Model	Expt.	Model
a	2.1	⋯	5458	130	137	⋯	0.9756
a	3.7	⋯	5602	240	240	⋯	0.9577
a	9	⋯	6017	540	551	⋯	0.9087
b	10	6125	6088	580	606	0.9053	0.9007
b	15	6475	6414	831	865	0.8716	0.8651
b	20	6793	6701	1057	1105	0.8441	0.8349
b	30	7350	7204	1465	1543	0.8008	0.7852
b	100	10 126	9573	3546	3873	0.6498	0.5939

[a]See Ref. 11.
[b]See Ref. 1.

limiting case, $C = c^+ = 5320$ m/s for $\nu^- = \nu^+ = 27$ m/s. This result compares well with $c_0 = c^+ + \nu^+ = 5380$ m/s, i.e., $c^+ = 5353$ m/s from Swegle and Grady.[16]

It is worth emphasizing that the results obtained in this section are independent of the viscous part of the material response specified in Eqs. (15) and (18). Results depend solely on the shape of the compression curve C_Y. This curve is governed by the elastic law Eqs. (11), (12) and the plastic hardening law Eq. (20). Material characteristics are provided by a single quasistatic elastic–plastic tensile test and by ultrasonic measurements to estimate the second order elastic constants.

B. Shock structure

The shock structure is obtained by integration of the differential equation (46). Results shown in Fig. 4 are for $\sigma^- = 3.7$ GPa and values of viscous parameters ($M = 1.78$, $T_1^* = 1.6$ MPa) as listed in Table I. The variation of λ_1, λ_1^p and

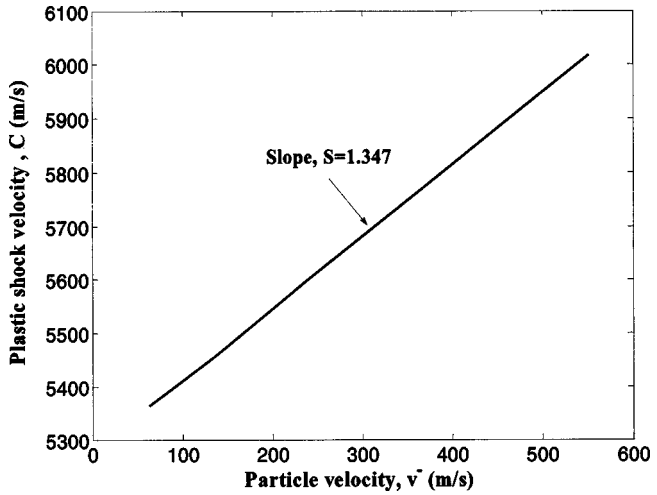

FIG. 3. Plastic shock velocity vs particle velocity ν^- at the rear of the plastic front. Values of the shock strength are in the range 2 GPa$\leqslant\sigma^-\leqslant$9 GPa. Note that the linear trend with slope $S = 1.347$ agrees with the value $S = 1.337$ identified by Swegle and Grady (Ref. 17), from experimental results.

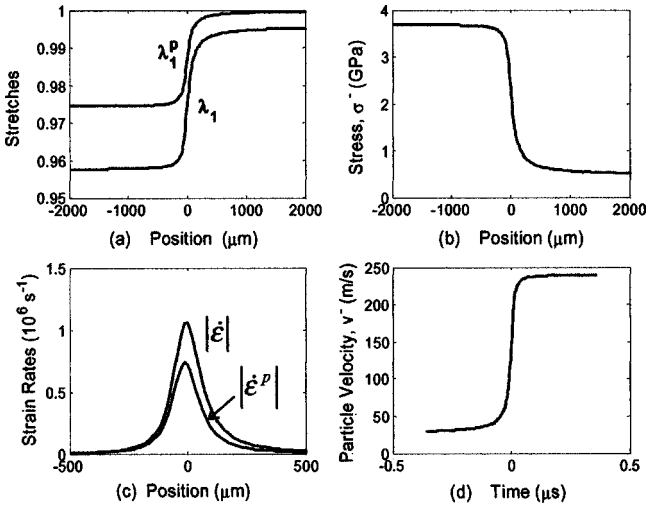

FIG. 4. Shock structure: (a) profile of the total stretch λ_1 and of the plastic stretch λ_1^p within the shock layer in terms of the position ξ, (b) profile of the compressive stress σ^-, (c) profile of the total and plastic strain rates, $|\dot{\epsilon}|$ and $|\dot{\epsilon}^p|$, respectively, and (d) particle velocity ν^- vs time.

of the compression stress σ with respect to ξ, are displayed in Figs. 4(a) and 4(b). Figure 4(c) shows the evolution of the total and the plastic strain rates, respectively, $\dot{\epsilon}$ and $\dot{\epsilon}^p$ (absolute values are shown). It appears that max $|\dot{\epsilon}|$ is about 40% larger than max$|\dot{\epsilon}^p|$. Figure 4(d) shows the particle velocity ν^- at the rear of the plastic front in terms of time. Such profiles have been recorded for aluminum by Johnson and Barker,[11] at different shock strengths ($\sigma^- = 2.1$ GPa, $\sigma^- = 3.7$ GPa, and $\sigma^- = 9$ GPa). It must be noted that for the largest stress level, $\sigma^- = 9$ GPa, the particle velocity measurements were made at the limit of the time resolution of the experimental setup available at that time.

In Fig. 5, the shock profiles (particle velocity ν^- versus time) are displayed for different values of the stress amplitude σ^-. Model predictions are compared to the experimental data of Johnson and Barker.[11] The good agreement that is evident is due to the appropriate choice of the parameters (M, T_1^*) controlling the viscous flow. A method to determine these parameters from the shock wave experimental data will be discussed in Sec. VI.

An interesting feature of the model is to provide an estimate of the shock width w_1. Considering Eq. (46), the following estimate is obtained:

$$w_1 = \frac{1-\lambda_1^{p-}}{\max(d\lambda_1^p/d\xi)} = \frac{3C}{2}\,\frac{1-\lambda_1^{p-}}{\max[\lambda_1^p \Phi_R(\lambda_1^p)]}. \tag{57}$$

This expression is the ratio of the variation of the plastic stretch $(1-\lambda_1^{p-})$ across the shock front, by a measure of the variation rate which is taken here as $\max(d\lambda_1^p/d\xi)$. To a very good approximation, the maximum of $\lambda_1^p \Phi(\lambda_1^p)$ occurs at the middle of the shock layer. This is verified by Fig. 6, where the variations of $\lambda_1^p \Phi(\lambda_1^p)$ and $\Phi(\lambda_1^p)$ are shown in terms of λ_1^p for the stress amplitude $\sigma^- = 3.7$ GPa. Furthermore, at the middle of the shock layer, the plastic stretch λ_1^p has nearly reached half of its variation and can be approximated by

$$\overline{\lambda_1^p} = (1/2)(1+\lambda_1^{p-}). \tag{58}$$

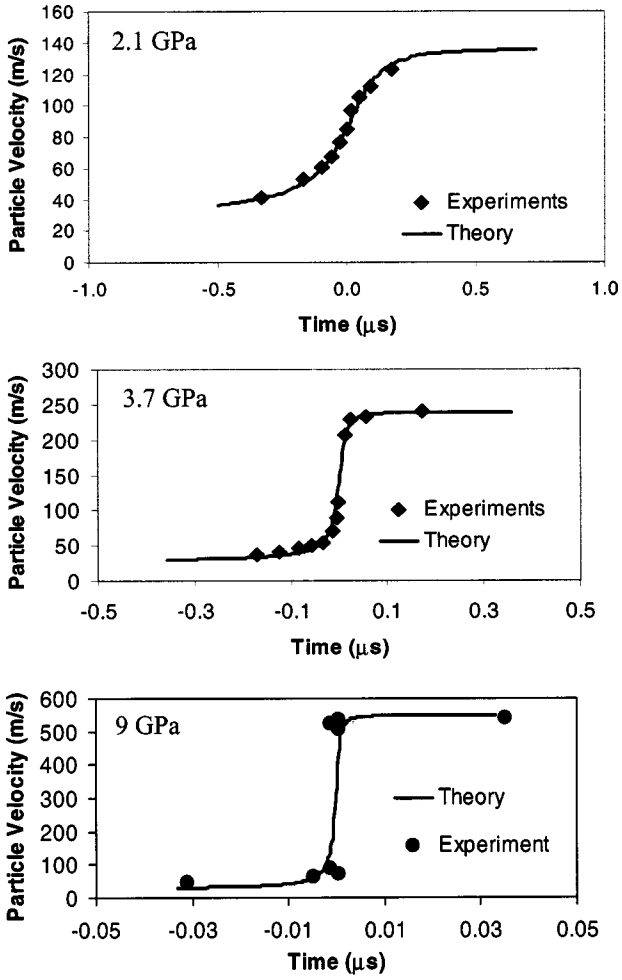

FIG. 5. Shock profiles showing the evolution of the particle velocity v^- with time, for different stress amplitudes, $\sigma^-=2.1$ GPa, $\sigma^-=3.7$ GPa, and $\sigma^-=9$ GPa. The model predictions are compared with experimental data for aluminum obtained by Johnson and Barker (see Ref. 11).

With these approximations, the shock width is characterized as

$$w_1^a \approx \frac{3C}{2}\frac{1-\lambda_1^{p-}}{\overline{\lambda_1^p \Phi_R(\lambda_1^p)}}. \tag{59}$$

Another estimate for shock width can be found by considering the following form of Eq. (46):

$$\frac{d}{d\xi}\ln(\lambda_1^p)=\frac{2}{3C}\Phi(\tau,\gamma^p). \tag{60}$$

from which one gets

$$w_2=\frac{3C}{2}\frac{\ln(1/\lambda_1^{p-})}{\max \Phi_R(\lambda_1^p)} \tag{61}$$

and the estimate

$$w_2^a=\frac{3C}{2}\frac{\ln(1/\lambda_1^{p-})}{\overline{\Phi_R(\lambda_1^p)}}. \tag{62}$$

For moderate deformations, $1-\lambda_1^p$ is a small quantity and the estimates Eqs. (59) and (62) provide very close results. For the loading, $\sigma^-=3.7$ GPa, one obtains

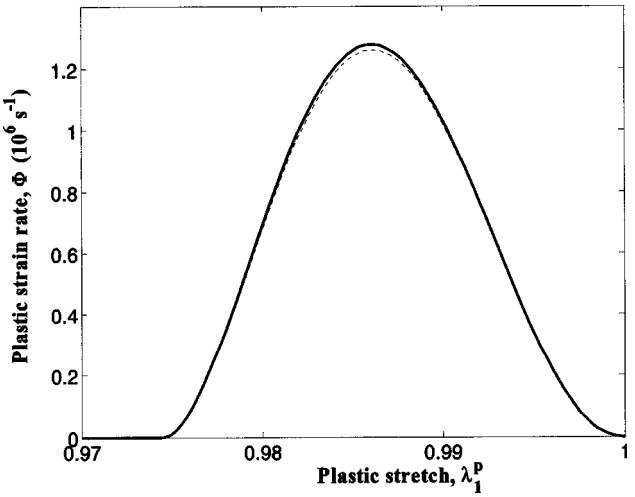

FIG. 6. Variation, within the shock layer, of the plastic strain rate $\dot{\gamma}^p=\Phi$ (continuous line) and of $\lambda_1^p\phi(\lambda_1^p)$ (dashed line) in terms of the plastic stretch λ_1^p. The shock stress amplitude is $\sigma^-=3.7$ GPa. Plastic flow vanishes at the states $(+)$ and $(-)$ corresponding, respectively, to $\lambda_1^{p+}=1$ and $\lambda_1^{p-}=0.9745$.

$$w_1^a \approx w_2^a = 196\ \ \mu\text{m}; \quad w_1^e \approx w_2^e = 201\ \ \mu\text{m}. \tag{63}$$

In Fig. 7, the evolution of the characteristic shock width w_1 is reported in terms of the shock amplitude σ^-. The value of w_1^a is also plotted but is almost indistinguishable from w_1. Two choices of the viscous parameters have been considered: (i) $(M,T_1^*)=(1.78,1.6\,\text{MPa})$ as in Table I, and (ii) $(M,T_1^*)=(2,2.33\,\text{MPa})$. Note that w_1 grows to very large values when the stress amplitude becomes smaller than 2 GPa [case (i) $w_1=10$ cm for $\sigma^-=1$ GPa]. Actually, from the expression Eq. (59) for the characteristic width, it follows

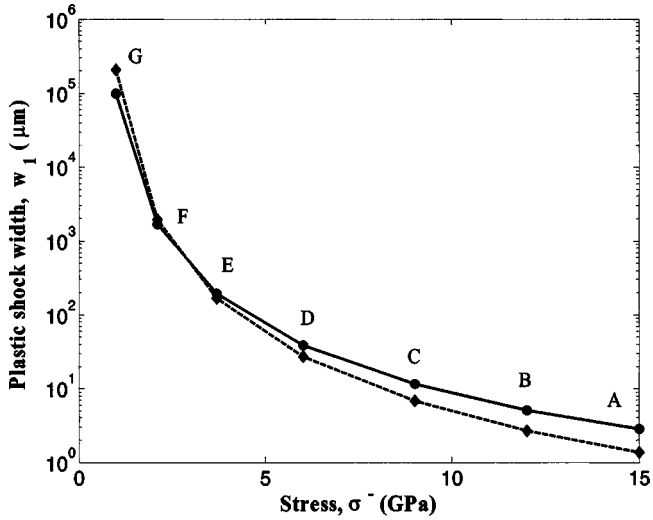

FIG. 7. Evolution of the characteristic shock width w_1 with the stress amplitude σ^-. Results for w_1^a are also reported on this figure, but they are hardly distinguishable from w_1. Two choices of the viscous parameters have been considered: (i) curve with circles, $(M,T_1^*)=(1.78,1.6\,\text{MPa})$ as in Table I and (ii) discontinuous curve with dots, $(M,T_1^*)=(2,2.33\,\text{MPa})$. The following values of $(\sigma^-\,(\text{GPa}),w_1\,(\mu\text{m}))$ are associated to the corresponding points (circles or dots): (i) $A=(15,2.80)$, $B=(12,5.09)$, $C=(9,11.5)$, $D=(6,39)$, $E=(3.7,196)$, $F=(2.1,1681)$, $G=(1,0.100\times10^6)$. (ii) $A=(15,1.36)$, $B=(12,2.7)$, $C=(9,6.8)$, $D=(6,27)$, $E=(3.7,171)$, $F=(2.1,1964)$, $G=(1,0.209\times10^6)$.

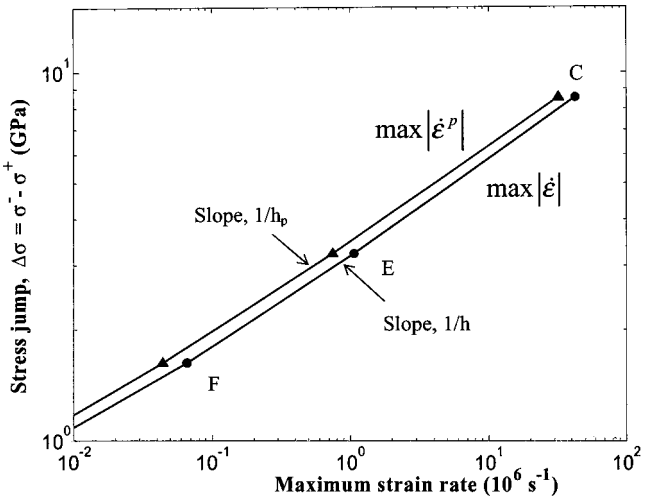

FIG. 8. Stress jump $\Delta\sigma=\sigma^- - \sigma^+$ across the shock layer in terms of $\max|\dot{\epsilon}^p|$ (dashed curve) and $\max|\dot{\epsilon}|$ (continuous curve). For the values of the material parameters given in Table I, $h=3.92$ and $h_p=3.98$ for the range of stress amplitudes considered in the experiments of Johnson and Barker (Ref. 11) ($\sigma^-=2.1$,3.7,9 GPa), with labels *F*, *E*, and *C* as in Fig. 7.

that $w_1^a \to \infty$ when $\sigma^- \to \sigma^+$ [since $\lambda_1^{p-} \to 1$, $\overline{\lambda}_1^p \to 1$, $\Phi(\overline{\lambda}_1^p) \to 0$]. According to Bland,[9] a propagation distance of at least five times the shock width is needed to achieve steady state conditions at the shock front. For $\sigma^-=1$ GPa this means that the specimen should be at least 50 cm thick! For $\sigma^-=3.7$ GPa, the thickness should be larger than 1 mm.

In Fig. 8, the stress jump $\Delta\sigma=\sigma^- - \sigma^+$ is given in terms of the quantities $\max|\dot{\epsilon}^p|$ and $\max|\dot{\epsilon}|$ evaluated within the shock layer (i.e., on the Rayleigh line), with $\dot{\epsilon}^p$ and $\dot{\epsilon}$ being, respectively, the longitudinal plastic strain rate Eq. (54) and the total strain rate Eq. (55). In the log–log plot of Fig. 8, two straight lines are obtained which are nearly parallel, suggesting the following laws:

$$\max|\dot{\epsilon}^p| = \beta_p(\Delta\sigma)^{h_p}, \tag{64a}$$

$$\max|\dot{\epsilon}| = \beta(\Delta\sigma)^{h}. \tag{64b}$$

The slopes of the lines in Fig. 8 are $1/h_p$ and $1/h$. It will be shown later that h_p and h depend on M but are not dependent on T_1^*, while β_p and β depend on both M and T_1^*. For the values of material parameters considered in Table I, $h=3.92$ and $h_p=3.98$. It is worth noting that the exponent of $\Delta\sigma$ from the present model agrees well with that identified by Swegle and Grady[16] from the experimental results of Johnson and Barker,[11] $h_{SG}=4$. However, the rate sensitivity parameter is $M=1/m=1.78$ in the present model, while it was $M=2$ in the approach developed by Swegle and Grady.[16] Further discussion of this issue is provided in Sec. VI.

V. CLOSED FORM SOLUTIONS FOR THE SHOCK STRUCTURE

For certain values of the strain rate sensitivity $m=1/M$, the differential equation (46) has an explicit closed form solution. It was shown before that on the Rayleigh line $\tau+\tau_a$ can be expressed in terms of the single variable λ_1^p. Using the notations of Fig. 2(a), the Rayleigh line intersects the compression curve C_Y at points J and K where $\lambda_1^p=1$ and $\lambda_1^p=\lambda_1^{p-}$. Since $\tau+\tau_a=0$ at J and K, one can approximate $\tau+\tau_a$ on the Rayleigh line by a linear dependence upon λ_1^p-1 and $\lambda_1^p-\lambda_1^{p-}$, respectively, in the vicinity of J and K. Taking into account the exponent M in expression (23) for the dislocation velocity, Φ can be approximated by the following function of λ_1^p:

$$\Phi(\lambda_1^p) = \frac{4^M \Phi_{\max}}{(1-\lambda_1^{p-})^{2M}} (1-\lambda_1^p)^M (\lambda_1^p - \lambda_1^{p-})^M. \tag{65}$$

The right hand side of Eq. (65) has been normalized to have the maximum $\Phi_{\max}$ of Φ at the mean value of the plastic stretch $\overline{\lambda}_1^p=(1/2)(1+\lambda_1^{p-})$, in accordance with results of Fig. 6. For a moderate deformation, the right hand side of Eq. (42) can be approximated by replacing $\lambda_1^p\Phi$ by $\overline{\lambda}_1^p\Phi$

$$\frac{d\lambda_1^p}{d\xi} = K(1-\lambda_1^p)^M(\lambda_1^p-\lambda_1^{p-})^M, \tag{66}$$

where

$$K = \frac{2\overline{\lambda}_1^p}{3C} \frac{4^M \Phi_{\max}}{(1-\lambda_1^{p-})^{2M}}. \tag{67}$$

The solution for the differential equation (66) has the form:

$$\xi = K^{-1}(1-\lambda_1^{p-})^{1-2M} Z[(\lambda_1^p-\lambda_1^{p-})/(1-\lambda_1^{p-})], \tag{68}$$

where Z is the function

$$Z(x) = \int \frac{dx}{(1-x)^M x^M} \quad (0 \leqslant x \leqslant 1). \tag{69}$$

When M is an integer, the integral Eq. (69) can be evaluated explicitly. For instance for $M=1$,

$$Z(x) = \ln\left(\frac{x}{1-x}\right), \tag{70}$$

and hence

$$\lambda_1^p = 1 + \frac{\lambda_1^{p-}-1}{2}\left[1 - \tanh\left(\frac{1-\lambda_1^{p-}}{2} K\xi\right)\right]. \tag{71}$$

Similarly for $M=2$,

$$Z(x) = 2\ln\left(\frac{x}{1-x}\right) - \frac{1}{x} + \frac{1}{1-x}. \tag{72}$$

The solutions corresponding to $M=1$ and $M=2$ are shown in Fig. 9, and compared to the numerical quadrature of Eq. (46). The closed form and numerical solutions are in good agreement, lending credence to the simplifying assumptions proposed here.

VI. PARAMETRIC ANALYSIS

In this section, the effects of material parameters on the shock structure are analyzed, with special emphasis on parameters characterizing the material rate sensitivity. An important question is how to relate experimental data (in particular, shock profiles) to the rate sensitivity characteristics. A key parameter associated with the shock structure is the

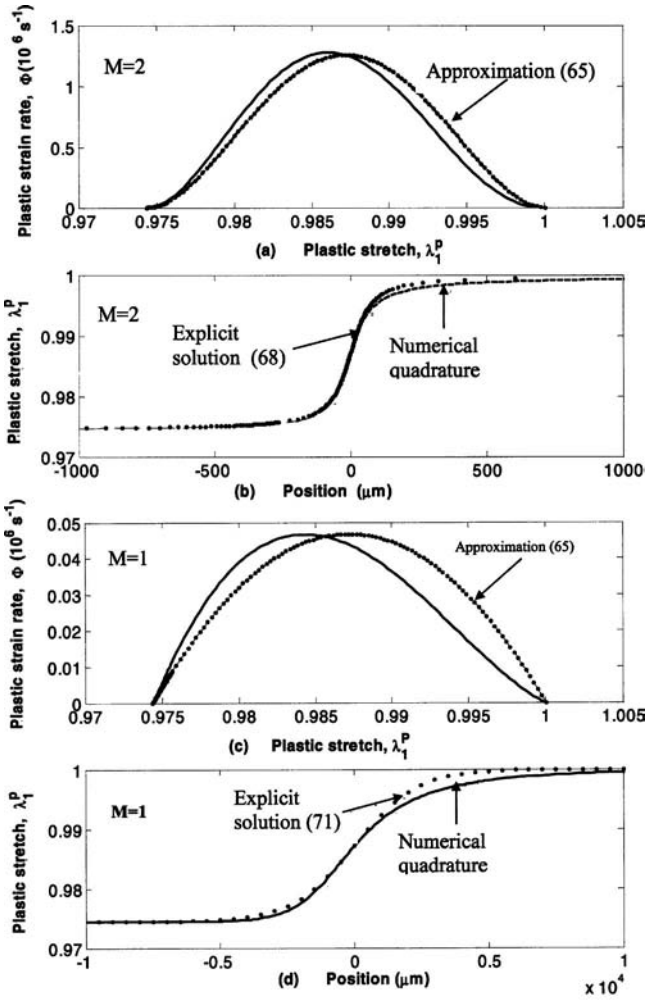

FIG. 9. The results shown here correspond to the following choice of the viscous parameters (a), (b) ($M=2$, $T_1^*=2.33$ MPa), (c), (d) ($M=1$, $T_1^*=2.33$ MPa). In (a) and (c) the evolution of the plastic strain rate $\Phi=\dot{\gamma}^p$ is given in terms of the plastic stretch λ_1^p. The approximation Eq. (65) is compared with the exact solution. In (b) and (c), the approximate solution (written in explicit form) is compared with the numerical quadrature of Eq. (46).

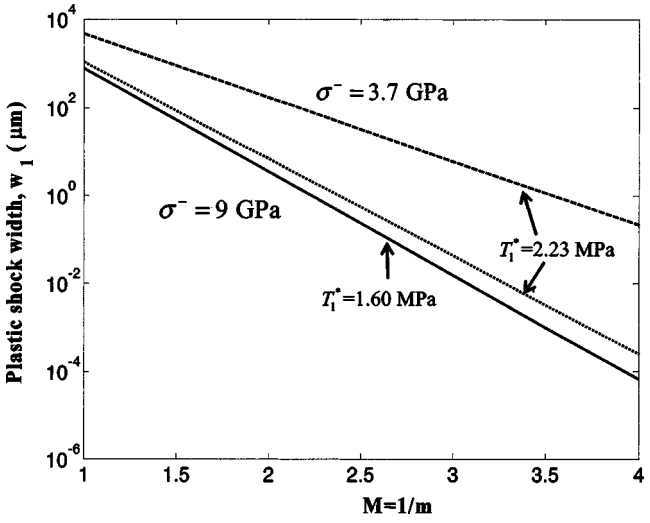

FIG. 10. Dependence of the characteristic shock width w_1 with respect to the rate sensitivity parameter $M=1/m$ for two values of the shock strength and two values of T_1^*. Results for w_1^a are not distinguishable from w_1 on this graph. Note that the linear dependence with respect to M, in this semilog diagram, reflects the power law dependence Eq. (74).

characteristic width defined by the relationships (57) or (59). Expressions (61) and (62) will not be considered since they give results very close to, respectively, Eqs. (57) and (59). Note first that the term $(3C/2)(1-\lambda_1^{p-})$ is entirely determined by the compression curve $C_Y:\lambda_1\rightarrow\sigma(\lambda_1)$ and by the loading amplitude (characterized by λ_1^- or by σ^-). Consequently, this term is not affected by the material strain rate sensitivity, as C_Y does not depend on the viscous response of the material. Indeed, viscous effects are embedded in the term $\max(\lambda_1^p\Phi_R(\lambda_1^p))$ with

$$\Phi_R(\lambda_1^p)=bNc_1\left(\frac{|\tau+\tau_a|}{T_1^*}\right)^M. \tag{73}$$

Using Eq. (59), the characteristic width can be written as

$$w_1^a\approx\frac{3C}{2}\frac{1-\lambda_1^{p-}}{\overline{\lambda_1^p}bN(\overline{\lambda_1^p})c_1(|\tau+\tau_a|/T_1^*)^M}, \tag{74}$$

where the denominator is evaluated in terms of the mean plastic stretch $\overline{\lambda_1^p}$ by using the relationship (53) established on the Rayleigh line. In Fig. 10 the characteristic shock width w_1 (not distinguishable from w_1^a when reported on the same graph) is given in terms of $M=1/m$ for two values of the shock strength $\sigma^-=3.7$ and 9 GPa. Due to the structure of the relationship (74), w_1^a shows a linear dependence with respect to M in the semilog scaling of Fig. 10. These results indicate that, by decreasing the strain rate sensitivity parameter m, i.e., by increasing $M=1/m$, the shock width is decreased in a significant proportion. Considering the material characteristics given in Table I, and the imposed stress $\sigma^-=9$ GPa, one obtains $w_1=11.5\,\mu$m for $M=1.78$, and $w_1=0.0153\,\mu$m for $M=3$, i.e., a variation of the shock width by a factor of 75.

In Fig. 11 the characteristic width, estimated by w_1 (or equivalently by w_1^a), is represented in terms of the reference stress T_1^* for the given stress amplitude $\sigma^-=3.7$ GPa, and two values of the rate sensitivity parameter $M=1.78$ and $M=2$. T_1^* was introduced in the viscoplastic law Eq. (23) and characterizes the resistance to viscous flow. In the log–log diagram of Fig. 11, the slope is given by M as a direct consequence of Eq. (74). In Sec. III B it was found that the maximum of the plastic strain rate $\max|\dot{\epsilon}^p|$ in the shock layer is related to the stress jump $\Delta\sigma=\sigma^--\sigma^+$ by a power law of the form Eq. (64a), where h_p is the exponent of $\Delta\sigma$. A similar relationship was found when considering the total strain rate $\dot{\epsilon}$ in place of $\dot{\epsilon}^p$, the exponent now being h. When the rate sensitivity parameter M varies, it is found that the relationships (64) are still valid, with the exponents h_p and h depending upon M as illustrated in Fig. 12. To a very good approximation, these exponents can be represented in terms of M by

$$h_p=1.87M+0.663 \tag{75a}$$

and

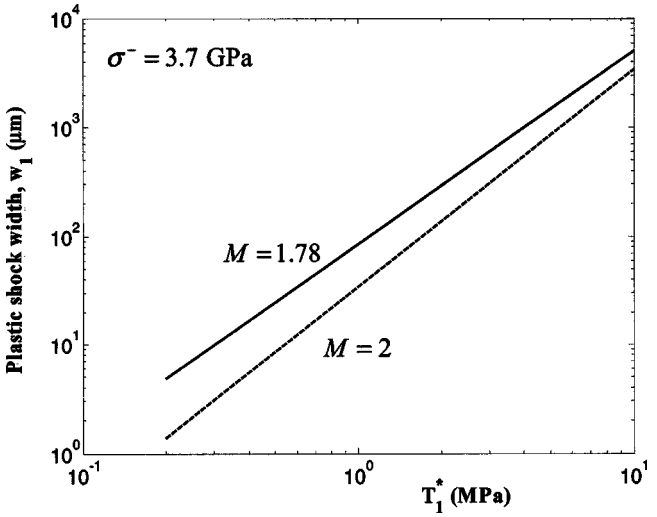

FIG. 11. Variation of the characteristic shock width w_1 with respect to the reference stress T_1^*, for the stress amplitude $\sigma^- = 3.7$ GPa and two values of the rate sensitivity parameter M. In this log–log diagram, the slope is given by M.

$$h = 1.87M + 0.620. \tag{75b}$$

Note that the value $h=4$ reported by Swegle and Grady[16] to be the best fit of experimental results for aluminum, corresponds to $M=1.78$ with Eq. (75a) and $M=1.81$ with Eq. (75b). Note also that the coefficients on the right hand side of Eq. (75) may depend upon other material parameters (elastic constants, etc.). The parameter T_1^* does not affect h and h_p, as illustrated by Fig. 13 where $\Delta\sigma$ versus $\max|\dot{\epsilon}^p|$ diagrams are shown for different values of T_1^*. To simplify the drawing, the dependence with respect to $\max|\dot{\epsilon}|$ is not represented, since the results are similar.

In Fig. 14, $\Delta\sigma$ is represented in terms of $\max|\dot{\epsilon}^p|$ for various values of M and T_1^*. For the fixed value $T_1^* = 1.6$ MPa, a family of straight lines is obtained when M is varied; these lines intersect at the point I. Similarly, the family of lines associated with $T_1^* = 100$ MPa intersect at point J.

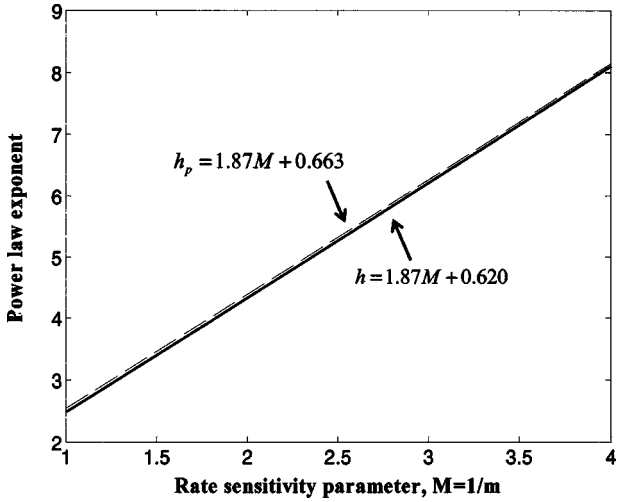

FIG. 12. Linear dependence of h_p and h [exponent of $\Delta\sigma$ in the power laws Eq. (64)] with respect to the rate sensitivity parameter $M=1/m$. The results are very well represented by $h_p = 1.87M + 0.663$ and $h = 1.87M + 0.620$.

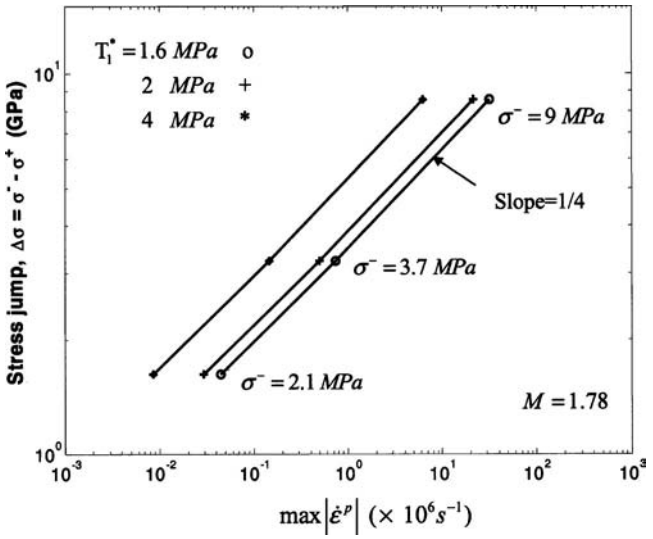

FIG. 13. Stress jump across the shock $\Delta\sigma = \sigma^- - \sigma^+$ vs $\max|\dot{\epsilon}^p|$, for various values of T_1^*. The slope $1/h_p$ is shown to be independent upon T_1^*. Similarly h is independent of T_1^*. Material parameters are those of Table I, except for $T_1^* = 2$ and 4 MPa.

Note that for a given value of M, a family of parallel lines is obtained when T_1^* varies, as seen in Fig. 13. The exponent h also depends on material parameters other than M, namely those which affect the shape of the isothermal compression curve. The values of the second order elastic constants a_4, a_5, a_6 have an important effect on h and h_p. For the material characterized in Table I, it was found that $h=3.92$ and $h_p=3.98$. By multiplying the values of a_4, a_5, a_6 given in Table I by 0.5, 2, and 10, one has, respectively ($h=4.15$, $h_p=4.20$), ($h=3.65$, $h_p=3.73$), and ($h=3.02$, $h_p=3.10$). The effect of the second order elastic constants on h is illus-

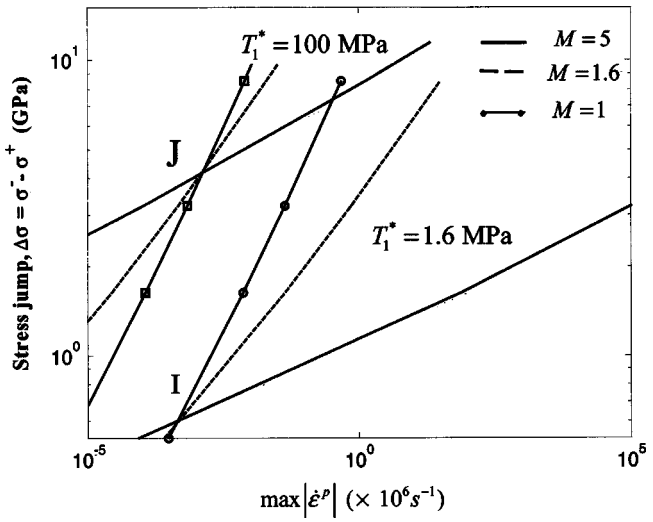

FIG. 14. Stress jump across the shock $\Delta\sigma = \sigma^- - \sigma^+$, vs $\max|\dot{\epsilon}^p|$, for various values of the viscosity parameters M and T_1^*. When M has a fixed value, and T_1^* is varied, parallel straight lines are obtained as in Fig. 13. For $T_1^* = 1.6$ MPa, a family of lines is obtained when M varies; these lines intersect at I. Similarly, for $T_1^* = 100$ MPa, a family of lines is obtained which intersect at J. A given choice of parameters M and T_1^*, corresponds to a line with slope $1/h_p$. This diagram illustrates the dependence of h_p upon M and T_1^*. Similar results are obtained when considering h.

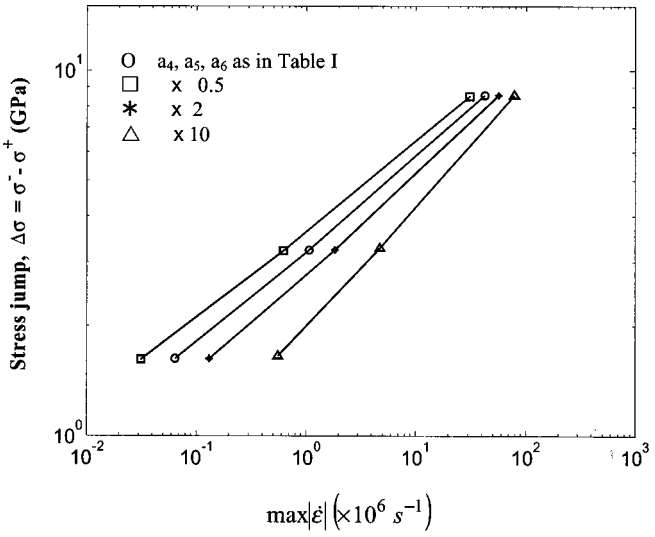

FIG. 15. Stress jump across the shock $\Delta\sigma=\sigma^{-}-\sigma^{+}$ vs $\max|\dot{\epsilon}|$ for various values of the parameters a_4, a_5, and a_6. While in Fig. 14 the plastic strain rate was considered, here the total strain rate $\dot{\epsilon}$ is used to illustrate the similarity of results. Material parameters are those of Table I. Different lines are obtained depending on the values chosen for the second order elastic constants a_4, a_5, and a_6. These values are those of Table I multiplied by 0.5 (squares), 1 (circles), 2 (stars), and 10 (triangles), respectively.

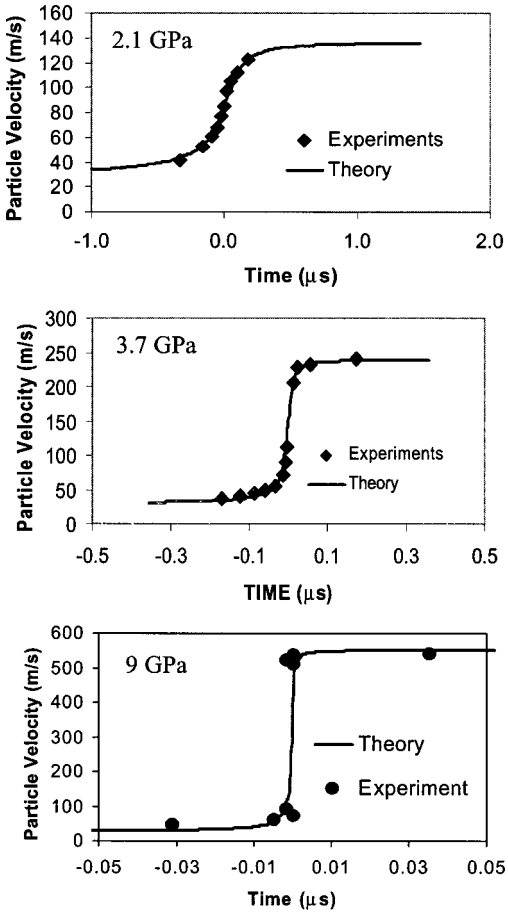

FIG. 16. As in Fig. 5, particle velocity v^{-} vs time plots are presented, for different stress amplitudes, $\sigma^{-}=2.1$, 3.7, and 9 GPa. The model results are compared with experimental data for aluminum obtained by Johnson and Barker (Ref. 11). Here the viscous parameters are $M=2$ and $T_1^*=2.23$ MPa. The comparisons are as good as in Fig. 5, where the following values were used: $M=1.78$ and $T_1^*=1.6$ MPa.

trated in Fig. 15. It is important to note that the curvature of the compression curve C_Y is affected by the values of the second order elastic constants. The curvature of C_Y can be quantified by the coefficient S introduced in Eq. (56). For the material parameters of Table I, it was found that $S=1.347$, while for a_4, a_5, a_6 multiplied by 0.5, 2, and 10, one has $S=0.954$, $S=2.02$, and $S=5.3$, respectively. For the broad class of materials considered by Swegle and Grady,[16] the values of S are in the range of 1.18–1.5, therefore it is imperative that the real values of a_4, a_5, a_6 must be in a limited range to be compatible with the measured values of S.

The structure of the shock front is governed mainly by the "viscous" response given by Eq. (23). In this law the yield limit is defined by the term $-\tau_a$. The viscous response is governed by two independent material parameters M and T_1^*; c_1 is not an independent parameter, since it can be embedded into T_1^*. The effects of parameters (M,T_1^*) on the shock structure can be examined by considering how they affect the characteristic shock width. The expression Eq. (74) for w_1 shows that for a given shock strength (i.e., for a given λ_1^{-} or a given σ^{-}), there exist an infinity of pairs (M,T_1^*) producing the same width. Considering two such couples, (M,T_1^*) and $(M',T_1^{*'})$, they are related by the relationship

$$\left(\frac{\overline{T}}{T_1^*}\right)^{M}=\left(\frac{\overline{T}}{T_1^{*'}}\right)^{M'}, \tag{76}$$

where $\overline{T}=|\tau+\tau_a|_{\overline{\lambda}_1^p}$ is evaluated on the Rayleigh line for the value $\overline{\lambda}_1^p$ of the plastic stretch. Therefore, calibrating the shock width does not provide a unique choice for the viscous parameters. However, (M,T_1^*) can be evaluated in an adequate way by calibration with the $(\max|\dot{\epsilon}|,\Delta\sigma)$ diagram. As shown in Fig. 14, the slope and the level of this plot is controlled, respectively by M and T_1^*. A further check is provided by the consideration of particle velocity versus time profiles as in Fig. 5. In Fig. 16, particle velocity versus time profiles predicted for $(M,T_1^*)=(2,2.233\,\text{MPa})$ are considered and it appears that experimental data are indeed well reproduced. This illustrates again the fact that the sole consideration of these shock profiles is not sufficient to provide a unique choice of the viscous parameters.

However, as discussed before, the value of the exponent h in Eq. (64b) provides an additional constraint for selecting appropriate values of (M,T_1^*). One obtains $(h=4.35,\ h_p=4.40)$ for $(M,T_1^*)=(2,2.23\,\text{MPa})$. The result $(h=3.92,\ h_p=3.98)$ found for the values listed in Table I, namely $(M,T_1^*)=(1.78,1.60\,\text{MPa})$ is in better agreement with the value $h=4$ estimated by Swegle and Grady[16] for aluminum.

VII. SUMMARY

Steady plastic shock waves observed in metals during plate impact experiments have been analyzed. Considering shocks of moderate amplitude, a simplified framework was adopted in which the process can be considered as quasi-

isentropic. Thermal effects have been evaluated and are shown to be negligible for the range of stress amplitudes considered here. Results were illustrated by choosing aluminum as the model material. Following Clifton,[17] the material response of aluminum is characterized via two different tests: elastic–plastic characteristics are taken from an isothermal tensile test and second order elastic constants are given by ultrasonic measurements.

Using a Lagrangian setting appropriate for large deformation, an analytical solution of steady plastic shocks has been formulated. This solution provides a clear insight concerning the effects of material parameters and loading conditions on the shock profile. In particular, an explicit formula has been obtained for the characteristic shock width. The effect of viscous like parameters governing the viscoplastic flow such as strain rate sensitivity and flow stress resistance on the shock profile have been analyzed. Conversely, the extraction of these viscous parameters from particle velocity profile measurements has been discussed. Hence, shock wave experiments could provide valuable information on the viscous response of materials subjected to very high loading rates, in addition to their traditional role of establishing their Hugoniot relations.

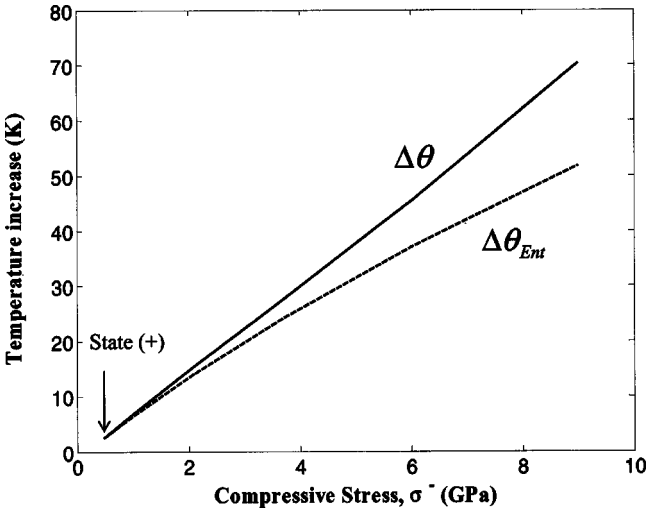

FIG. 17. Variation of the temperature increase $\Delta\theta$ in terms of the compression stress σ^-; $\Delta\theta=\theta-\theta_0$ (continuous curve) is calculated at the rear of the plastic front, state $(-)$; θ_0 is the initial ambient temperature. $\Delta\theta$ is the superposition of two contributions, $\Delta\theta=\Delta\theta_{\text{Plast}}+\Delta\theta_{\text{Ent}}$ where $\Delta\theta_{\text{Ent}}$ (dashed curve) represents the thermoelastic effect (or entropic effect), and $\Delta\theta_{\text{Plast}}$ is the temperature increase due to the dissipation of part of the plastic work into heat. The temperature increase at the rear of the elastic precursor, state $(+)$, $\Delta\theta=2.46$ K, is entirely due to the thermoelastic effect. Material parameters are those of aluminum given in Table I.

ACKNOWLEDGMENTS

The research reported here was supported by the Army Research Office (Dr. B. LaMattina, Program Manager), which is gratefully acknowledged. G.R. acknowledges the support of DOE through Caltech's ASCI/ASAP Center for the Simulation of Dynamic Response of Materials.

APPENDIX A: SECOND ORDER ELASTIC CONSTANTS

The function F_1 introduced in Eq. (11) is defined as[17]

$$F_1(\epsilon_1^e,\epsilon_2^e,\epsilon_3^e)=a_1+2a_2(\epsilon_1^e+\epsilon_2^e+\epsilon_3^e)+a_3(\epsilon_2^e+\epsilon_3^e)+3a_4(\epsilon_1^e+\epsilon_2^e+\epsilon_3^e)^2+\ldots+a_5[(\epsilon_1^e+\epsilon_2^e+\epsilon_3^e)(\epsilon_2^e+\epsilon_3^e)+(\epsilon_1^e\epsilon_2^e+\epsilon_2^e\epsilon_3^e+\epsilon_3^e\epsilon_1^e)]+a_6\epsilon_2^e\epsilon_3^e. \tag{A1}$$

F_2 appearing in Eq. (12) is obtained from F_1 by interchanging ϵ_1^e and ϵ_2^e, and by changing a_1 into $\hat{a}_1$

$$F_2(\epsilon_1^e,\epsilon_2^e,\epsilon_3^e)=F_1(\epsilon_2^e,\epsilon_1^e,\epsilon_3^e). \tag{A2}$$

If initial stresses are equal to zero (which is the case in the present article), one has

$$a_1=0,\quad \hat{a}_1=0. \tag{A3}$$

Because of axisymmetry, F_1 and F_2 can be evaluated by setting $\epsilon_3^e=\epsilon_2^e$. Therefore one can write

$$F_1(\epsilon_1^e,\epsilon_2^e)=a_1+A_1\epsilon_1^e+A_2{\epsilon_1^e}^2+B_1\epsilon_2^e+B_2{\epsilon_2^e}^2+D\epsilon_1^e\epsilon_2^e, \tag{A4}$$

where

$$A_1=2a_2,\quad A_2=3a_4,$$
$$B_1=4a_2+2a_3,\quad B_2=12a_4+5a_5+a_6,\quad D=12a_4+4a_5. \tag{A5}$$

The values of the coefficients a_i are given in Table I for aluminum; a_1 and $\hat{a}_1$ are related to the initial stresses. The second order thermoelastic constants a_4, a_5, and a_6 have been identified with ultrasonic measurements.[17] Note that expression (A1) of F_1 is only valid for isentropic transformations. A general expression of F_1 and F_2, including entropic terms, is given by Clifton.[17]

APPENDIX B: DERIVATIVE OF g_R

The derivative of g_R with respect to λ_1^p can be written as

$$g_R'(\lambda_1^p)=1+f(X)+(1/2)(1+X)f'(X), \tag{B1}$$

where

$$X=(\lambda_1^p)^{1/2}-1, \tag{B2}$$

$$f'(X)=-\frac{B'}{2A_2}+\frac{1}{4A_2}\frac{2BB'-4A_2G'}{\sqrt{B^2-4A_2G}}, \tag{B3}$$

$$B'=dB/dX=D-4C^2(1+X)^3, \tag{B4}$$

$$G'=B_1+2B_2X+2(C^2\lambda^++\sigma^+/\rho_0)(1+X)-4C^2(1+X)^3. \tag{B5}$$

APPENDIX C: EFFECT OF TEMPERATURE

The variation of temperature $\Delta\theta$ is due to the superposition of two contributions. The compression of a solid produces a temperature rise $\Delta\theta_{\text{Ent}}$, similar to the heating of a gas under adiabatic compression, which is the thermo–elastic effect (or entropic effect). For isentropic conditions

$$\Delta\theta_{\mathrm{Ent}} = b_1(\epsilon_1^e + 2\epsilon_2^e) + b_2(\epsilon_1^e + 2\epsilon_2^e)^2 + b_3(\epsilon_1^e + 2\epsilon_2^e)\epsilon_2^e, \tag{C1}$$

where ϵ_1^e and ϵ_2^e are the elastic strains defined in Eqs. (13) and (14), and b_1, b_2, b_3 are thermo–elastic constants given in Table I.[17] The second contribution is related to the dissipation of mechanical work related to the physics of plastic deformation. Considering that a proportion β_{TQ} (Taylor–Quinney coefficient) of the plastic work W_p is dissipated into heat, the following contribution to the temperature increase is obtained:

$$\Delta\theta_{\mathrm{plast}} = \beta_{\mathrm{TQ}} W_p / \rho_0 C_p, \tag{C2}$$

where C_p is the specific heat at constant pressure. The rate of plastic work is given by[17]

$$\dot{W}^p = -\tfrac{4}{3}\lambda_1 \tau \phi. \tag{C3}$$

Finally, by superposition the temperature variation with respect to the initial ambient temperature θ_0 is obtained

$$\Delta\theta = \theta - \theta_0 = \Delta\theta_{\mathrm{Ent}} + \Delta\theta_{\mathrm{plast}}. \tag{C4}$$

In Fig. 17, $\Delta\theta$ is plotted at the rear of the plastic shock, state $(-)$, in terms of the stress amplitude σ^-, for aluminum with material properties given in Table I. For $\sigma^- = \sigma^+ = 0.473\,\mathrm{MPa}$, the plastic shock does not exist; $\Delta\theta = 2.46$ K is the temperature increase (solely due to the thermoelastic effect) at the rear of the elastic precursor, state $(+)$. For $\sigma^- = 9\,\mathrm{GPa}$, one obtains $\Delta\theta = 70$ K. This temperature increase does not affect the mechanical response of aluminum ($T_{\mathrm{melt}} = 933\,\mathrm{K}$) significantly. Therefore, having neglected the effect of the temperature in the present model is justified for shocks of moderate amplitude.

[1] M. H. Rice, R. G. McQueen, and J. M. Walsh, in *Solid State Physics*, edited by F. Seitz and D. Turnbull (Academic, San Diego, 1958), Vol. 6, p.1.
[2] S. P. Marsh, *LASL Shock Hugoniot Data* (University of California Press, Berkeley, CA, 1980).
[3] Lord Rayleigh, Proc. R. Soc. London **84**, 247 (1910).
[4] G. I. Taylor, Proc. R. Soc. London **84**, 371 (1910).
[5] W. Band, J. Geophys. Res. **65**, 695 (1960).
[6] W. Band and G. E. Duvall, Am. J. Phys. **29**, 780 (1961).
[7] D. R. Bland, J. Inst. Math. Appl. **1**, 56 (1964).
[8] L. M. Barker, in *Behavior of Dense Media Under High Dynamic Pressures* (Gordon and Breach, New York, 1968), p. 483.
[9] V. N. Mineev and E. V. Savinov, Sov. Phys. JETP **25**, 411 (1967).
[10] V. N. Mineev and R. M. Zaidel, Sov. Phys. JETP **27**, 874 (1968).
[11] J. N. Johnson and L. M. Barker, J. Appl. Phys. **40**, 4321 (1969).
[12] R. Manvi, G. E. Duvall, and S. C. Lowell, Int. J. Mech. Sci. **11**, 1 (1969).
[13] G. W. Swan, G. E. Duvall, and C. K. Thornhill, J. Mech. Phys. Solids **21**, 215 (1973).
[14] F. E. Prieto and C. Renero, J. Appl. Phys. **44**, 4013 (1973).
[15] S. K. Godunov, A. A. Deribas, and V. I. Mail, Combust., Explos. Shock Waves **11**, 3 (1975).
[16] J. W. Swegle and D. E. Grady, J. Appl. Phys. **58**, 692 (1985).
[17] R. J. Clifton, in *Shock Waves and the Mechanical Properties of Solids*, edited by J. J. Burke and V. Weiss (Syracuse University Press, Syracuse, N.Y., 1971), p. 73.
[18] P. Perzyna, Adv. Appl. Math. **9**, 243 (1966).